34th Annual International Conference of the IEEE EMBS
San Diego, California USA, 28 August - 1 September, 2012

Fully Automated Segmentation of the Left Ventricle Applied to Cine MR Images: Description and Results on a Database of 45 Subjects

Constantin Constantinidès, Elodie Roullot, Muriel Lefort, and Frédérique Frouin, *Member, IEEE*

***Abstract*— A fully automated segmentation method of the left ventricle from short-axis cardiac MR images is proposed and evaluated. The segmentation is based on morphological filtering and gradient vector flow snake for which an automatic setting of parameters has already been proposed. The present work focuses on the automatic detection of a region of interest (ROI) surrounding the left ventricle, prior to the segmentation step. The whole process was applied to the MICCAI 2009 Left Ventricle Challenge database containing 45 subjects (9 healthy subjects and 36 with pathology). The automatic detection of the ROI was judged accurate in 86% of the cases. It failed in 2% of the slices and provided an overestimation in 9% of the slices. Furthermore, the endocardial segmentation was accurate in 80% of the slices and the epicardial was judged satisfactory in 71% of the slices. This fully automated procedure can thus be used as a first step in a user controlled approach, in order to reduce the total number of interactions.**

I. Introduction

Many segmentation approaches have been proposed for cine short-axis cardiac magnetic resonance (MR) images. For instance, a recent review [1] selected 70 such methods, published on this topic. Our concern was to consider the applicability of methods in a clinical context. Due to its specific role in the blood circulation and to its pathological occurrences, the left ventricle (LV) is largely studied, pathologies of right ventricle being less frequent. One current goal of clinical MR studies is to obtain a reliable estimation of parameters that are useful for the current diagnosis or follow-up, such as end-diastolic volumes (EDV), end-systolic volumes (ESV), ejection fraction (EF), and myocardial mass (MM). For these reasons, our approach was deliberately focused on 3D segmentation of the left ventricle, rather than on a 4D segmentation, including the temporal dimension. To estimate the above mentioned parameters, the endocardium of the left ventricle was segmented at end-diastolic and end-systolic phases. Furthermore, the epicardium was segmented at end-diastolic phase. The segmentation process was based on a previously developed semi-automated approach [2], for which the feedback was positive when compared to other existing methods [3]. But this method requires, for each slice, the definition by the user of a rectangular region of interest (ROI) including the left ventricle.

Recently, we proposed different attempts to make this preliminary step more automatic. The first one was applied at the "on line contest" of the Cardiac MR Left Ventricle Challenge (MICCAI challenge) [4] but still required some initialization through the definition of a parallelepiped box including the left ventricle). Moreover, it proved to be too simple. The second one [5] was fully automatic, but showed more than 20% of misplaced regions. Reasons for these misplaced regions were analyzed and led us to propose an improved version, presented here.

The fully automatic method was applied to the 45 data-sets of the MICCAI database [4]. To evaluate it in a standard way and to have a performance tracking system comparable to other teams, we first applied the evaluation code that was provided by the organizers of the MICCAI challenge and used the reference provided for this challenge. Furthermore, the clinical parameters EDV, ESV, EF, and MM were computed using customized software. Moreover, to measure the gap between the fully automated method and the semi-automatic technique [2], results are given for both approaches.

II. Methods

A. Basics of the semi-automatic and the automatic approaches

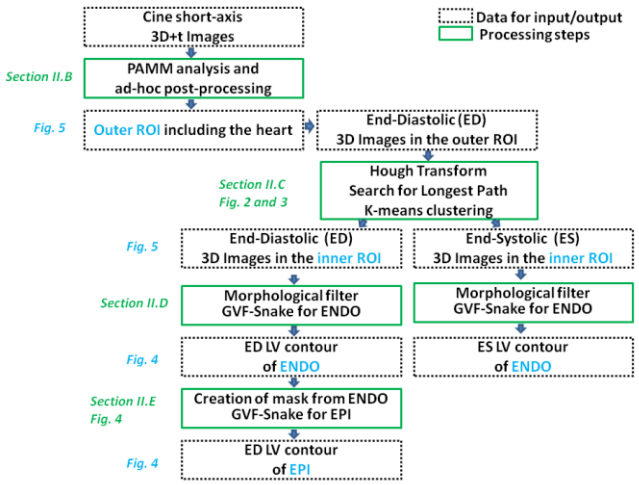

Figure 1. Flowchart of the fully automatic segmentation approach. ENDO stands for the endocardium and EPI for the epicardium.

The semi-automatic method as described in [2] required the manual definition of a rectangular ROI including the LV. Inside this ROI, a preprocessing step consisted of a set of morphological filters using different values of the size parameter (from 5 to 80 % of the size of the ROI) and of an automatic choice of the size parameter. Then the filtered image was segmented using a gradient vector flow (GVF) snake with *a priori* set values for its parameters. Depending

C. Constantinidès, M Lefort, and F Frouin are with Inserm at University Pierre et Marie Curie, Paris, France (corresponding author: F. Frouin, phone: +33 1 53 82 84 00; fax: +33 1 53 82 84 48; e-mail: frouin@imed.jussieu.fr).

C. Constantinidès, and E Roullot are with ESME-Sudria, Ivry-sur-Seine, France.

on the quality of results, some slices could be segmented again using a different size parameter for the morphological filter and/or modified values of the GVF-snake parameters, implying additional user inputs.

The automated steps of the previous approach (morphological filtering and GVF snake, with no "second chance" segmentation) were retained for the fully automated approach. In addition, the definition of the ROI including the LV was made fully automatic. Fig. 1 shows the general pipeline of the method, each step being further detailed in next subsections.

B. Automatic detection of the cardiac region

The detection of the cardiac region is based on the assumption that the heart is subject to motion whereas the other regions remain still during one cardiac cycle. The Parametric Analysis of Main Motion (PAMM) method [6] was thus applied to "3D+t" cine images, $S(v,t)$, v being a voxel and t the cardiac phase. PAMM models this dynamic volume of images by a non linear function of four 3D parametric images: $A1(v), A2(v), Tb(v), Te(v)$,

$$S(v,t) = A1(v) - A2(v) f(t, Tb(v), Te(v)) + e(v,t),$$

with $f(t) = 1$ if $Tb(v) \leq t \leq Te(v), f(t) = 0$ else. (1)

$A1$and $A2$ respectively correspond to the constant grey level and to the varying component of S during the cardiac cycle, whereas Tb and Te are time values respectively corresponding to the beginning and the end of the local motion of contraction. They are estimated in order to minimize the error $e(v,t)$. A threshold equal to three times the mean grey level in $A2$ was applied to this 3D amplitude image $A2(v)$ and 3D connected sets were extracted from the resulting binary volume. The biggest connected set was considered as the one associated to the cardiac structure. The smallest parallelepiped box including this largest set was defined as the cardiac region [5].

C. Automatic detection of the left ventricular region

This step was performed in order to estimate a smallest region including the LV, and excluding as much as possible adjacent structures (the right ventricle, the liver or the lungs). This was necessary to make the next steps (morphological filtering and GVF-snake segmentation) more efficient. A circular Hough transform [7] was applied to each end-diastolic slice restricted to the previously defined region of interest. We configured this procedure in order to detect several circles on each slice and allow the detection of concentric circles. It is thus highly sensitive but not specific enough for the detection of the LV. To detect LV, two simple rules were tested [5]. The first one computed the maximum intensity projection (MIP) of the detected circles, and the circles with the closest centers to the maximum of MIP image were selected. The second one was based on the *a priori* knowledge that the grey level within the left ventricular cavity should be high (high mean value m) and homogeneous (low standard deviation σ). A mixed criterion $h = m/\sigma$ was thus computed for each circle, the circle having the largest criterion h was finally selected for each slice.

Using the first rule, the number of misplaced regions reached 33%; using the second rule, it was equal to 22%. Interestingly, the misplaced regions were different using the two rules, showing the advantage of making them cooperate to reduce this number of misplaced regions. Extending the idea exploited with the MIP rule, a 3D tracking of centers of circle was implemented. Using graph formalism, each center of circle formed a vertex. The value h was associated to each vertex, retaining the smallest circle in case of several concentric circles detected for one vertex. Directed edges from the apex towards the base were drawn to link pairs of vertices belonging to two consecutive slices, under the condition that the distance between projections of the two vertices in the same short axis plane be less than 10 pixels. Vertices from which no edge could be drawn towards the next slice were considered for linking with vertices of the following slice. Once the graph was completed, the sum of the vertex weights h was computed for each path and the path with the highest value was selected. The corresponding circles were then selected on each slice (Fig. 2).

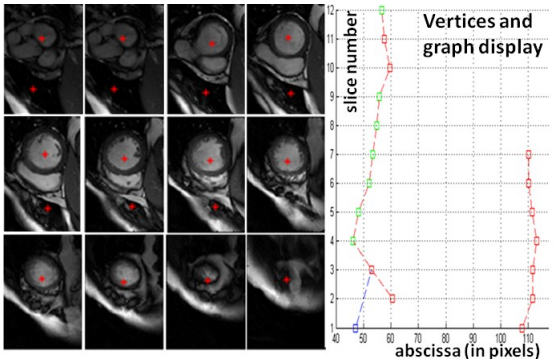

Figure 2. Centers of circles (red crosses) detected by the circular Hough transform on twelve consecutive slices. Corresponding graph and path detection: one in the LV (detected as optimal) and one in the lungs.

In some slices, the path was inside the cardiac structure but with possible centers in the septum or in the right cavity. Thus an additional refinement was systematically applied. Inside the box including the circle, a fuzzy k-means procedure was performed searching for two classes: a low intensity class associated to the myocardium, the lungs and possibly the pillar, and a high intensity class associated to the left and possibly the right cavities [8]. Connected sets associated to the high intensity class were labeled and the center of mass of the largest one was assumed to be the center of the left cavity and was noted P_0. Consistency of P_0 points estimated on adjacent slices was finally checked to ensure a 3D continuity of these points. The rectangular box including this connected set provided the final ROI surrounding the left ventricle, within which further segmentation of end-diastolic and end-systolic images was performed (Fig. 3).

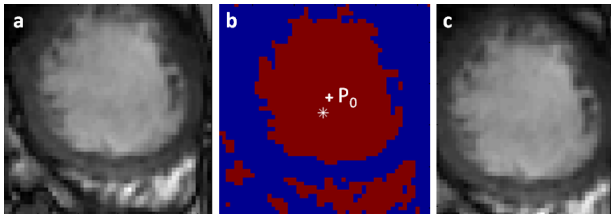

Figure 3. a) ROI obtained after searching for the optimal 3D path. b) classes estimated by the k-means procedure c) cropped image within the final ROI, centered in P_0

D. Segmentation of the endocardium

The conventional slice by slice approach that was developed for the semi-automated approach including morphological filtering and GVF-snake [2] was applied with automated detection of the size parameter for the morphological filter, and GVF-snake using *a priori* set parameters (Fig. 4). A small circle (3 mm radius) centered in P_0 was used as the initial snake C. The snake evolution was driven by its internal energy and external energy (2). Internal energy was controlled by two parameters, α and β, weighting respectively the elasticity and the rigidity of the snake. The external energy was a function of the pressure parameter κp applied to the normal of the snake N and the weight κ associated to the gradient vector flow. The gradient vector flow V_μ was estimated from the image gradient using a regularization parameter μ.

$$\int_0^1 \left[\alpha \left|\frac{\partial C}{\partial s}\right|^2 + \beta \left|\frac{\partial^2 C}{\partial^2 s}\right| + \kappa_p N(s) + \kappa_p V_\mu(s)\right] ds. \qquad (2)$$

The same set of parameters was defined for end-diastolic and end-systolic images: $\alpha = 1, \beta = 40, \kappa p = 0.8, \kappa = 1.7, \mu = 0.2$

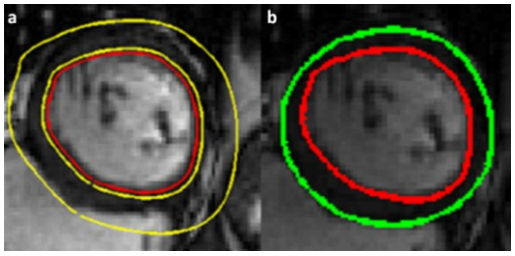

Figure 4. a) Segmentation of the endocardium (in red color) and definition of the mask (in yellow color) for the estimation of the epicardium b) resulting segmentation of the epicardium (in green color).

E. Segmentation of the epicardium

The segmentation the epicardium was based on the previous segmentation of the endocardium: the search region was limited to a ring mask inside which the contour points were estimated. Inner border was defined automatically at a distance of 2.5 mm of the endocardial contour and outer border at a distance of 20 mm (Fig. 4). Then GVF-snake segmentation was applied using the inner contour as initialization, each contour point going outside the mask being replaced by its nearest point on the mask border. Once again, parameters were set *a priori*, according to (3):

$$\alpha = 1 \quad \beta = 40 \quad \kappa p = 0.35 \quad \kappa = 1.7 \quad \mu = 0.2. \qquad (3)$$

F. Evaluation criteria

A manual delineation by experts was provided in the framework of the MICCAI Challenge. This contour was considered as the reference to compute the performance measures defined for the MICCAI Challenge using the code provided by the organizers. Thus, the percentage of "good contours" (for which the average perpendicular distance is less than 5 mm), the average perpendicular distance and the Dice index were reported for each patient. Each measure was computed slice per slice and a mean value for all the slices was finally given. However these two latter parameters were only computed for "good contours". To overcome this limitation, clinical parameters including EDV, ESV, EF, and MM were computed using all available contours. They were estimated using customized software.

III. Results

A. Automatic detection of the ROIs

The extraction of the cardiac ROI and of the left ventricular ROI was visually assessed in order to check the first steps of the automatic procedure.

TABLE I. Visual Assessment of Automatically Defined ROI

Percentage	Type of Regions of Interest	
	Cardiac	***Left Ventricular***
misplaced	0%	2%
too small	3%	3%
too large	78%	9%
correct	19%	86%

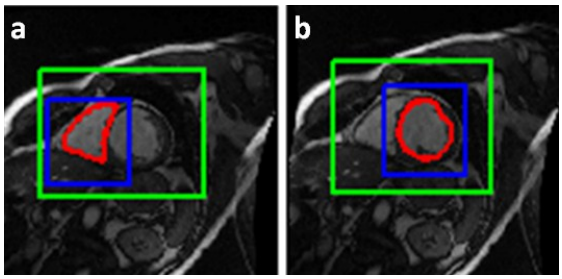

Figure 5. Examples of outer ROI surrouding the cardiac region (green box) and inner ROI (blue box). Associated segmentation of the endocardium (in red color) a) misplaced inner ROI resulting in the segmentation of the right ventricle, b) succesful segmentation.

B. Automatic and semi-automatic segmentation methods

Results are extensively given for both segmentation approaches in order to make the comparison easier.

Tables II and III give the percentage of "good contours", the mean average perpendicular distance, and the Dice index that were computed for each patient (mean ± standard deviation, [min-max]) as they are estimated using the evaluation software provided by MICCAI organizers.

TABLE II. Imaging Critria for the Endocardium

Percentage	Type of segmentation	
	Semi-automated	***Fully automated***
% of good contours	91±8 [61-100]	80± 16 [29-100]
APD (mm)	1.94±0.42 [1.17-3.03]	2.44 ±0.56 [1.31-4.20]
Dice index	0.89±0.04 [0.80-0.96]	0.86 ±0.05 [0.72-0.94]

TABLE III. Imaging Critria for the Epicardium

Percentage	Type of segmentation	
	Semi-automated	***Fully automated***
% of good contours	91±10 [70-100]	71 ±26 [0-100]
APD (mm)	2.38±0.57 [1.28-3.79]	2.80 ±0.71 [1.37-4.88]
Dice index	0.92 ± 0.02 [0.84-0.95]	0.91 ±0.03 [0.81-0.96]

The clinical parameters EDV, ESV, EF, and MM obtained by both approaches were compared them to the reference values using linear regression and Bland-Altman analysis. Tables IV, V, VI, and VII synthesize these results and provide the slope (a), the intercept at the origin (b), the correlation coefficient (r) of the regression analysis, and the bias ± standard deviation of the Bland-Altman plot.

TABLE IV. END-DIASTOLIC VOLUMES

Comparison with reference	Type of segmentation	
	Semi-automated	***Fully automated***
Regression analysis	a=0.99, b=-1.25, r=0.99	a=0.95, b=-3.23, r=0.96
Bias ± SD	2.65 ± 14.92 ml	11.82 ± 23.06 ml

TABLE V. END-SYSTOLIC VOLUMES

Comparison with reference	Type of segmentation	
	Semi-automated	***Fully automated***
Regression analysis	a=0.98, b=-5.96, r=0.99	a=0.91, b=-8.54, r=0.98
Bias ± SD	7.86 ± 12.47 ml	19.51 ± 20.12 ml

TABLE VI. LEFT VENTRICULAR EJECTION FRACTION

Comparison with reference	Type of segmentation	
	Semi-automated	***Fully automated***
Regression analysis	a=1.03, b=0.021, r=0.94	a=0.96, b=0.095, r=0.91
Bias ± SD	-0.034 ± 0.074	-0.076 ± 0.089

TABLE VII. MYOCARDIAL MASS

Comparison with reference	Type of segmentation	
	Semi-automated	***Fully automated***
Regression analysis	a=1.20, b=-13.61, r=0.91	a=0.38, b=46.79, r=0.44
Bias ± SD	-11.68 ± 25.85 g	31.43 ± 43.45 g

IV. DISCUSSION

The method that we proposed in this paper was to define automatically a ROI around the left ventricle in order to further segment it using GVF-snakes on filtered images. To achieve it, *a priori* information related to the cardiac motion, the circular shape of left cavity on short-axis slices, and spatial continuity between slices was used. This approach was applied to a database containing 45 patients for which contours drawn by an expert were available. All results indicate that the fully automated approach is very promising: the number of "good contours" (contours having an average perpendicular distance less than 5 mm) reaches 80% for the endocardium, including diastolic and systolic phases, and is superior to 70% for the epicardial contours.

Compared to our previous works, the improvement brought by this new automatic approach is substantial. Indeed, the definition of the ROI around the left ventricle is accurate in 86% of the slices, with a drastic reduction of misplaced regions - 2% when compared to more than 20% reported in [5]. The definition a 'too large' ROI, which occurs in 9% of the cases, is problematic for the further steps of the algorithm; indeed the choice of the size parameter in the morphological filtering can yield erroneous contours.

Of course the evaluation shows that the semi-automated approach works better, which is due to the authorized modification of parameters in case of incorrect contours. Due to its low computing time (about one minute per patient using a source code in Matlab® which could be optimized), this fully automated approach could be used as an initial segmentation. For instance, it can be combined with the semi-automated approach for clinical research applications. Previous work comparing three manual and five automated segmentation methods [3] has shown that our semi-automated method, although being 2D, was the closest to experts' performance. Thus the prior run of the fully automated approach will help to reduce the number of user interactions, since only few slices per patient need to be reworked.

Moreover, to improve the quality of the fully automated approach, some ideas are currently under investigation. The most promising consists in defining the size of the mask for the epicardial segmentation specifically for each patient. Indeed, it could yield a better estimation of this contour for hypertrophic patients (having a larger myocardium) or patients having a cardiac remodeling due to heart failure.

ACKNOWLEDGMENT

The authors thank the MedIEval group from the GdR Stic-Santé, GdR 2647 CNRS/Inserm, for providing customized software that computes clinical parameters from contours.

REFERENCES

[1] C Petitjean and JN Dacher, "A review of segmentation methods in short axis cardiac MR images" *Med Image Anal* , vol 15, 2011, pp. 169-84.

[2] R El Berbari et al. "Automated estimation of regional mean transition times and radial velocities from cine magnetic resonance images: evaluation in normal subjects." *J Magn Reson Imaging* , vol 30, 2009, pp.236-42.

[3] J Lebenberg et al. "Non-supervised ranking of different segmentation approaches. Application to the estimation of the left ventricle ejection fraction from cardiac cine MRI sequences." *IEEE Trans Med Imag* 2012, in press.

[4] P Radau et al. "Evaluation framework for algorithms segmenting short axis cardiac MRI." The MIDAS Journal - Cardiac MR Left Ventricle Segmentation Challenge, 2009: http://hdl.handle.net/10380/3070.

[5] C Constantinides et al. "Automated heart localization for the segmentation of the ventricular cavities on cine magnetic resonance images" in *Proc Computing in Cardiology*, vol 37, 2010, pp.911-4.

[6] C Ruiz-Dominguez et al. "Assessment of left ventricular contraction by parametric analysis of main motion (PAMM): theory and application for echocardiography" *Phys Med Biol* , vol 50, 2005, pp. 3277-96.

[7] D.H. Ballard, "Generalizing the Hough Transform to Detect Arbitrary Shapes" *Pattern Recognition* , vol 13, 1981, pp. 111-22.

[8] N. Kachenoura, et al. "Robust assessment of the transmural extent of myocardial infarction in late gadolinium-enhanced MRI studies using appropriate angular and circumferential subdivision of the myocardium." *Eur Radiol* , vol 18, 2008, pp. 2140-2147.